Energy Technology & Environmental Science

Synthesis and Optimization of a Highly Stable and Efficient BN/TiO_2 Nanocomposite for Phenol Degradation: A Photocatalytic, Mechanistic and Environmental Impact Study

Shekhah A. Al-Kandari,[a] Ahmed M. Mohamed,[a] Aboubakr M. Abdullah,*[b] Douaa S. AlMarzouq,[c] Gheyath K. Nasrallah,[d, e] Mohammed A. Sharaf,[f] Nadine Younes,[e] Munia M. Hamdan,[e] Talal Altahtamouni,[g] and Halema A. Al-Kandari*[c]

Different BN/TiO_2 nanocomposites were prepared hydrothermally, and their ratio was optimized to get the best photocatalytic performance towards phenol degradation. They were characterized by x-ray photoelectron spectroscopy, x-ray diffraction, Fourier transform infrared spectroscopy, thermal gravimetric analysis, scanning and transmission electron microscopies coupled with energy dispersive x-ray units, BET surface area, and UV-Vis diffuse reflectance. The bandgap energy was reduced from 3.35 to 2.95 eV due to the formation of the B–O–Ti bond. This allowed the exploitation of the visible light and inhibited the TiO_2 e^-/h^+ recombination, and consequently, the photocatalytic activity of TiO_2 was dramatically improved. Almost 90% mineralization of 20 ppm phenol solution was achieved within 30 min under simulated sunlight. The as-prepared composite showed excellent stability and reusability. Mechanistic analysis indicated that $O_2^{\cdot-}$ and h^+ played a crucial role in phenol degradation. The nanocomposite's biocompatibility and environmental impact were evaluated by analyzing its potential toxicity in vivo using the zebrafish embryos. 96-hpf acute toxicity assays, including the mortality rate assay (to obtain the LC50 values) and teratogenic assays (to obtain the No Observed Effect Concentration, NOEC) was conducted. The LC50 value for BN/TiO_2 was 482.5 mg L^{-1}, and the NOEC was 100 mg L^{-1}. Based on LC50 value and according to the Fish and Wildlife Service (FWS) acute toxicity rating scale, the photocatalyst is "practically not toxic."

Introduction

Wastewater treatment and reuse have become crucial in most arid societies. Many technologies are employed for wastewater treatment, such as biological digestion and chemical oxidation. However, photocatalysis is targeted for treating refractory pollutants and converting them to CO_2 and H_2O.[1] Titanium dioxide is one of these semiconductors widely tested as a photocatalyst due to its non-toxicity and photostability. Nevertheless, TiO_2 is limited in industrial applications due to its low photocatalytic activity and high bandgap energy. Many researchers showed that the performance of TiO_2 could be improved through coupling it with another semiconductor and/or nonmetals like nitrogen and carbon material. This can be attributed to the activity-defect relationship. For example, it was shown that N-doped TiO_2 nanotubes (TiON-NTs) have better photocatalytic performance than un-doped TiO_2 due to

[a] *Dr. S. A. Al-Kandari, Dr. A. M. Mohamed*
Chemistry Department, Faculty of Science,
Kuwait University,
P.O. Box 5969 Safat, 13060, Kuwait
[b] *Dr. A. M. Abdullah*
Center for Advanced Materials,
Qatar University, Doha, P.O. Box
2713, Qatar
E-mail: bakr@qu.edu.qa
[c] *Dr. D. S. AlMarzouq, Prof. H. A. Al-Kandari*
Department of Health Environment,
College of Health Sciences, PAAET, P.O. Box 1428,
Faiha 72853, Kuwait
E-mail: ha1.alkandari@paaet.edu.kw
[d] *Dr. G. K. Nasrallah*
Department of Biomedical Science,
College of Health Sciences, QU Health, Qatar
[e] *Dr. G. K. Nasrallah, N. Younes, M. M. Hamdan*
Biomedical Research Center Qatar University,
Qatar University,
Doha, P.O. Box 2713, Qatar
[f] *Prof. M. A. Sharaf*
Department of Maritime Transportation Management Engineering,
İstanbul University-Cerrahpaşa,
Avcilar, Istanbul 34320, Turkey
[g] *Prof. T. Altahtamouni*
Materials Science and Technology Program,
College of Arts and Sciences,
Qatar University,
Doha, P.O. Box 2713, Qatar

Supporting information for this article is available on the WWW under https://doi.org/10.1002/slct.202004820

merging the p-state of N-atoms with the O2p-state of TiO_2.[2] Besides, the photocatalytic activity of TiO_2 could be enhanced by coupling it with another metal such as Au, Pt.[2b,3] This enhancement in the photocatalytic activity referred to the Schottky junction formed between the TiO_2-NTs and metal nanoparticles which accelerated the charge transfer and depressed the electron-hole recombination. It was recently shown that iridium nanoparticles sensitized titanium oxynitride nitride nanotubes have better photocatalytic activity toward water splitting than TiON-NTs TiO_2-NTs due to high nitrogen-vacant concentration, larger size vacancy cluster, and small void of vacancy defects.[2b] Our research group showed that coupling TiO_2 with reduced graphene oxide or carbon nitride produced composites that efficiently degrade various organic compounds under sunlight.[4] Recently, more attention is being paid nowadays for the hexagonal boron nitride (h-BN), which is known as white graphene because it resembles graphene with its 2D arrangement. It consists of covalently-bonded boron and nitrogen organized in a honeycomb structure. It has an ample bandgap energy of 5.5 eV with exceptional electronic features.[5] Many researchers presented different preparation methods of pure BN and its composites and their photocatalytic applications.[5–6] Sing et al. obtained 79% degradation of 10 ppm methylene blue in 200 min on BN/TiO_2 .[7] Lui et al. evaluated the performance of BN/TiO_2 on rhodamine B and phenol. They achieved complete mineralization of rhodamine B and around 83% degradation of phenol after 10 h and 30 h irradiation, respectively.[5]

Although very few groups studied the photocatalytic activities of BN/TiO_2, our work's novelty is evident in many aspects. First, we optimized the ratio between the BN and the commercial P25 TiO_2 in the BN/TiO_2 nanocomposite to achieve the highest photocatalytic activity towards the degradation of 20 ppm phenol using visible simulated sunlight. This was achieved by changing and controlling the ratio and measure the photocatalytic activity using different experimental parameters. Second, a mechanistic study was done using different scavengers for the different photogenerated charge carriers. This helped us to understand the primary charge carrier involved in the degradation of phenol. Third, our preparation method is different as we used the hydrothermal treatment technique, which was never reported earlier for the BN/TiO_2. This method resulted in the formation of a nanocomposite rather than a physical mixing of the two components. The nanocomposite formation was proved from the measured bandgap energy as it was reduced to 2.95 rather than 3.35 and 5.95 eV for TiO_2 and BN, respectively. Fourth, the photocatalytic nature of the optimized nanocomposite was tested for phenol degradation rather than the simple dyes models that other groups report. Contrary to the dyes, phenol is a refractory water contaminant compound that is highly resistant to the different treatment types compared to the dyes. Fifth, our achievement is unique in terms of the period needed for almost a complete phenol degradation, where ~91% was degraded entirely in 30 minutes, and ~87% complete mineralization of phenol to CO_2 and water was achieved. Moreover, the as-prepared photocatalyst's cyclic use was also done, and the photocatalyst is proved to be highly stable. Seventh, the Zebrafish embryo model, a widely accepted model for toxicity assessment,[8] was exploited to evaluate any potential acute toxicology effect of BNTiO_2 never done in any previous study. Thus, an optimal BNTiO_2 nanoparticle concentration with the highest efficiency and minimal environmental impact on marine organisms and ecosystems of the marine environment can be recommended based on this study.

Results and discussion

Characterization

Figure 1 shows the SEM and TEM micrographs for the 2BNTi nanocomposite. It reveals the difference in BN size (40 nm) and TiO_2 (21 nm) nanoparticles. On the other hand, the HRTEM images of 2BNTi and the EDS mapping of the same nanocomposite are shown in Figure 2. The lattice fringes for both TiO_2 (0.35 nm) and BN (0.48 nm) are shown in Figure 2b. Also, the High-angle annular dark-field (HAADF) images are shown in Figure 2c, which clearly shows the atomic number's variation between the different components of the nanocomposite. Figure 2d is the EDS mapping, which confirms the four elements in the nanocomposite, B, N, Ti, and O. The TGA measurements of the 2BNTi is presented in Figure 3 under a nitrogen atmosphere from the room temperature to 800 °C. The depreciation in the weight percentage as the temperature increases is attributed to the adsorbed water vapor and gases' desorption. Only a reduction of 2% is noticed as the temperature increased up to 800 °C, which confirms the high thermal stability of the BNTi nanocomposite photocatalyst.

The FTIR spectra of pure BN, TiO_2, and after the composite synthesis (BNTi) are depicted in Figure 4. Two characteristic absorption bands of hexagonal BN (h-BN) were observed at 1320 and 806 cm^{-1}, corresponding to the stretching and bending modes of sp^2 hybridized BN skeletons, respectively.[6f,9] A broad band at 3228 cm^{-1} can be assigned for O–H from adsorbed water molecules on the surface of the sample and/or NH_2 groups, and absorption bands at 1515 are attributed to N–H bonds.[9a] A TiO_2 showed a peak at 1633 cm^{-1}, which can be assigned for deformed water molecules or a Ti–O–Ti stretching vibration, besides a full and broad absorption band below 1000 cm^{-1} corresponding to Ti–O–Ti vibration was observed.[4a,b] After loading BN on TiO_2, all absorption bands remain except that at 806 cm^{-1}, which overlaps with the strong absorption band of TiO_2 (Ti–O–Ti below 1000 cm^{-1}).

X-ray diffraction patterns of BN, BNTi, and TiO_2 were displayed in Figure 5. As shown from Figure 5, BN exists in a hexagonal shape with main characteristic peaks at 2 theta of 26.7 and 41.5° corresponding to 002 and 100 planes, respectively.[5,7,9a,d] In addition to the main peaks of h-BN, the characteristic peaks of the tetragonal anatase and rutile phase of TiO_2 were observed on BNTi nanocomposite. The characteristic peaks of TiO_2 anatase phase (JPDS21-1272) located at $2\theta =$ 25.4, 37.9, 48.0, 54.0, 55.1, 62.8, 69,1, 70.5, and 75.2°, while the peaks located at $2\theta = 27.5$, 36.1 and 41.1° are designated for rutile phase of TiO_2 (JPDS21-1276).[4a]

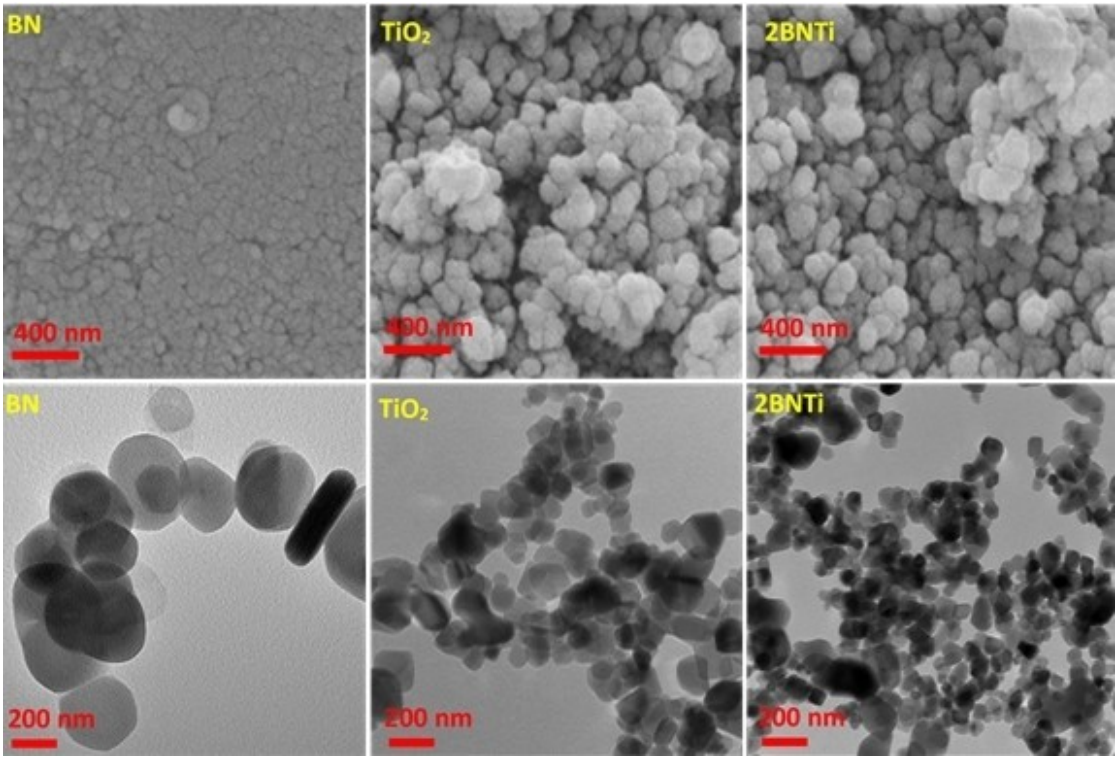

Figure 1. SEM (top) and TEM (below) micrographs for BN, TiO_2, and 2BNTi.

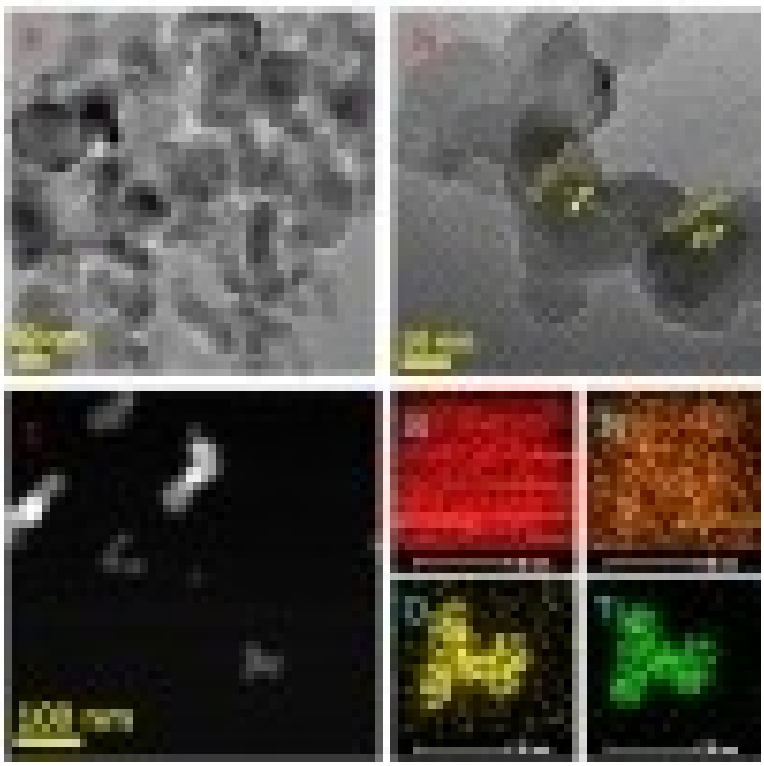

Figure 2. HRTEM (a and b) and HAADF (c) micrographs of 2BN/TiO2 and EDS mapping for B, N, Ti, and O.

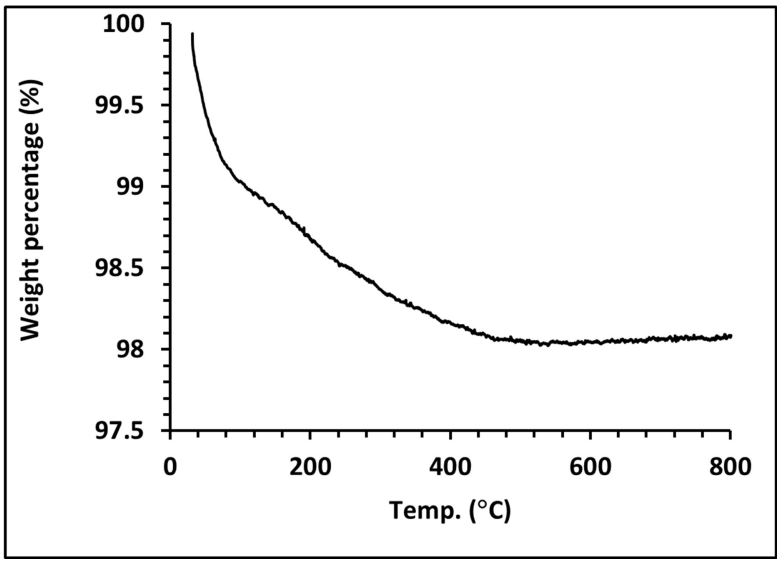

Figure 3. Thermogravimetric behavior of BN/TiO_2 nanocomposite.

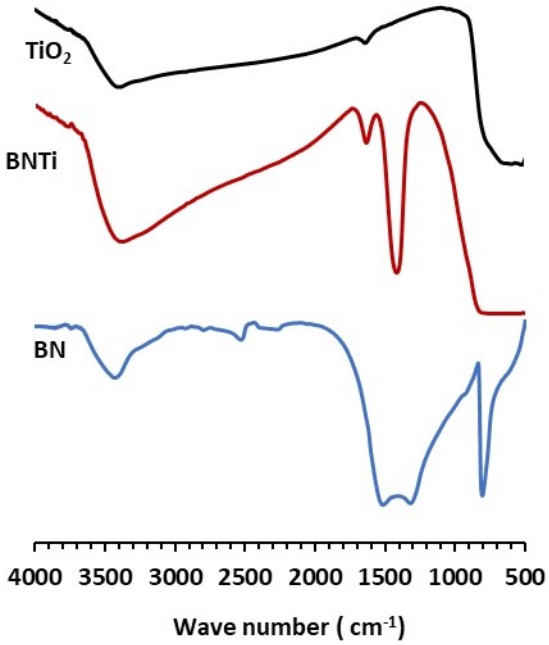

Figure 4. FT-IR spectra for BN, BNTi, and TiO_2.

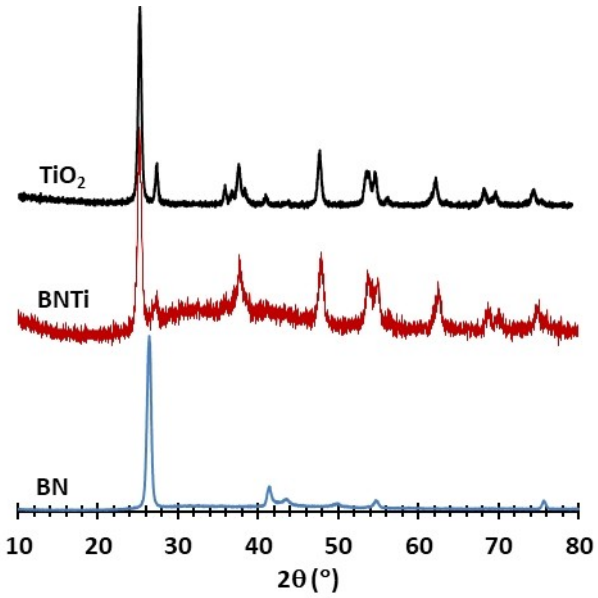

Figure 5. XRD for BN, 2BNTi, and TiO_2

XPS full survey spectra in the range of 0–1250 eV for TiO_2, BN, and BNTi are presented in Figure 6. The survey spectrum of TiO_2 showed the presence of three elements Ti, O, and C. In BN, two major peaks of N1s, B1s, and small amounts of O1s and C1s were observed (Figure 6A). The presence of O1s at 532.6 eV is due to the adsorbed water or O_2 species on BN's surface (Figure 6B),[6f] while the two peaks for O1s of the TiO_2 were noticed at 529.8 and 530.7 eV. The former peak is due to the Ti–O bond, and the latter is assigned to the –OH group.[10] However, the O1s peak at 530.8 eV in BNTi could be for –OH or B–O–Ti. The survey spectrum of BNTi showed the existence of N1s and B1s beside Ti2p and O1s on the surface of TiO_2, which revealed that BN was loaded successfully on TiO_2. On the other hand, the presence of C1s in survey spectra is due to the adventitious carbon. The XPS narrow scan of the N1s region at 390 to 410 eV (Figure 6 C) showed N1s at 398.1 and 398.2 eV in BN and BNTi, respectively. This result confirms that nitrogen atoms are bonded to B atoms (B–N)[6f] without any interaction with TiO_2. On the other hand, a small shoulder peak at 191.2 eV was observed beside the main peak at 190.5 eV for B1s after BN was loaded on TiO_2 (Figure 6D). The major peak at 190.5 eV is due to the B–N bond,[5,6f] while the shoulder peak is mostly due

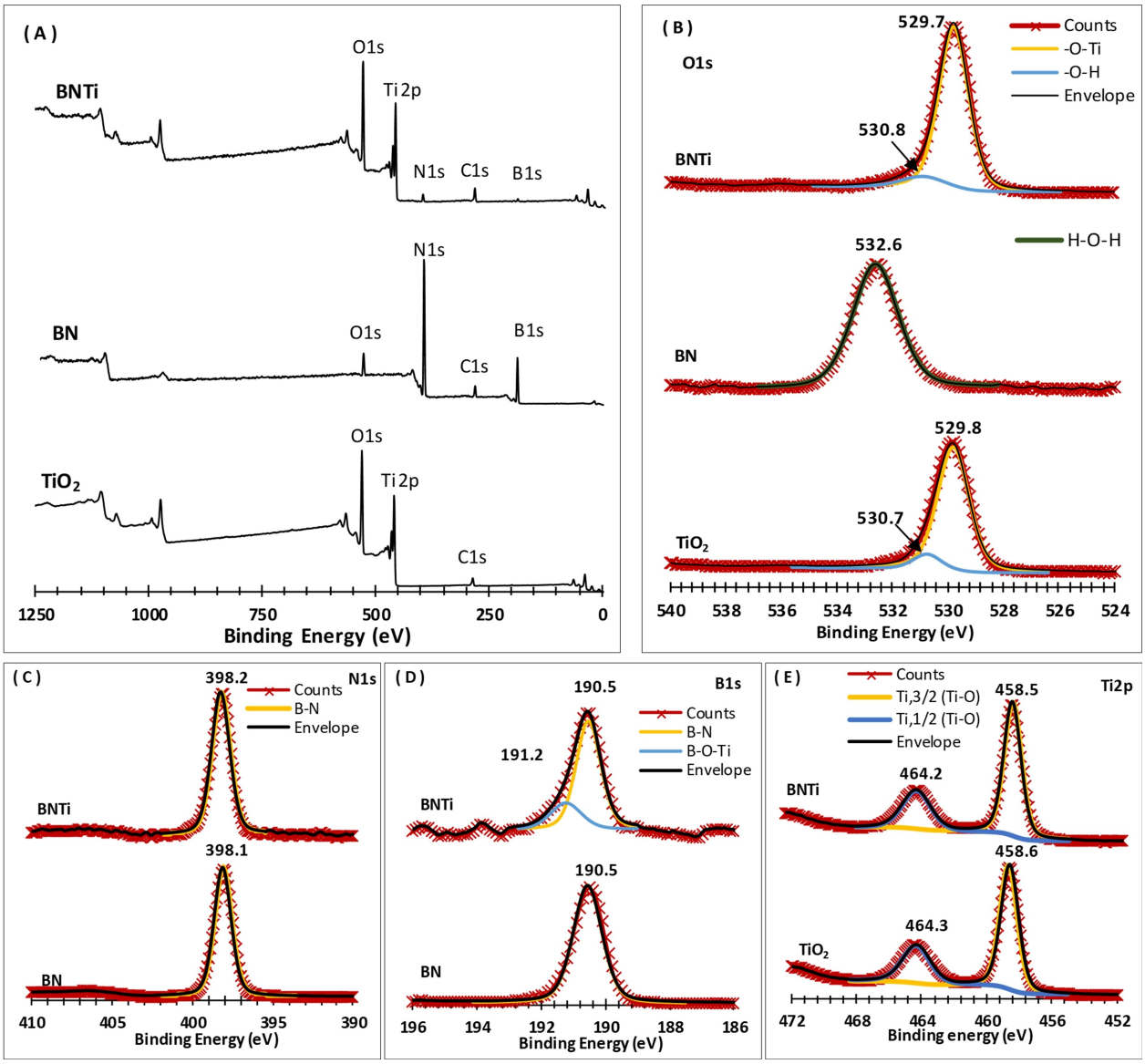

Figure 6. (A) XPS survey of TiO_2, BN, and BNTi, (B) O1s region of TiO_2, BN and BNTi, (C) N1s region of BN and BNTi, (D) B1s region of BN and BNTi and (E) Ti2p region of TiO_2 and BNTi

to the B–O–Ti,[11] which confirms a nanocomposite formation rather than a physical mixing between BN and TiO_2. There is no noticeable change in the binding energy and formation of new peaks in the Ti2p region, only Ti2p, 3/2, and Ti2p, 1/2 at 458.5, and 464.2 eV, respectively, was observed before and after loading BN on TiO_2 (Figure 6E). This result confirms the presence of Ti^{4+} and no bond formation between either B or N with Ti.

The UV-Vis spectroscopy with the diffuse reflectance unit was used to measure bandgap energy for the bare TiO_2 and BNTi nanocomposite, which corresponds to the wavelengths at the absorption edge. As shown in Figure 7, the bandgap energy of TiO_2 of 3.35 eV corresponding to 371 nm is reduced to 2.95 eV, equivalent to 422 nm. Therefore, it can be concluded that the loading of BN on TiO_2 shift the absorption wavelength of TiO_2 from the UV to the visible region, and the use of sunlight as an irradiation source becomes feasible. Note that the BET surface of bare BN and TiO_2 are measured to be 22 and 50 $m^2 g^{-1}$, respectively, and 47 $m^2 g^{-1}$ for 2BNTi, which indicates that the surface area did not play a significant role in the photocatalytic reactions under study.

photocatalytic experiments

Based on characterization results, we used a Xe lamp as an irradiation source to simulate sunlight. We notice no phenol degradation in the absence of photocatalyst (TiO_2 or BNTi), and bare BN has no catalytic activity toward phenol degradation. The photocatalytic degradation of 20 ppm phenol on TiO_2 and BNTi in the absence and presence of H_2O_2 was studied

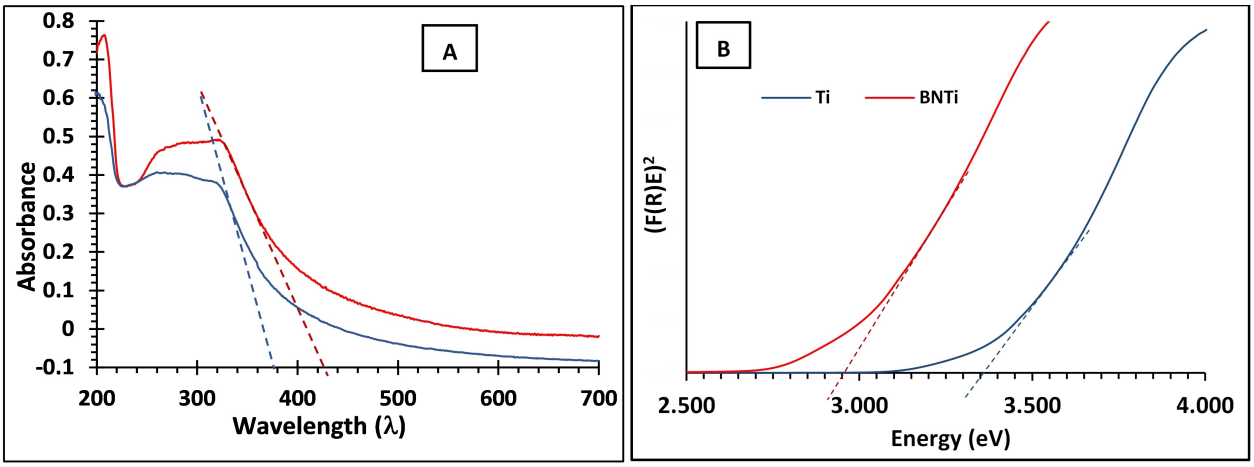

Figure 7. UV spectra (A) and corresponding bandgap energy (B)for Ti and 2BNTi nanocomposite.

(FigureA&B). The following conclusions can be extracted from Figure 8A **firstly, the rate of phenol increases with time in both cases. Secondly, the addition of H_2O_2 increases the rate of phenol degradation in both cases due to the increase in the hydroxyl radical generated during the reaction:**[4a]

$$H_2O_2 + e^-_{CB} \rightarrow {}^{\bullet}OH + OH^- \quad (1)$$

$$H_2O_2 \rightarrow {}^{\bullet}OH + {}^{\bullet}OH \quad (2)$$

Finally, the rate of phenol degradation is more pronounced on the BNTi nanocomposite compared with TiO_2 in the absence and presence of H_2O_2. A 90.2% degradation of phenol within 30 min in the presence of 70 μL H_2O_2 on BNTi is obtained. It is interesting to note that the rate of phenol degradation on BNTi without the addition of H_2O_2 fit well pseudo-first-order (Ln $\frac{C_t}{C0} = -Kt$) while pseudo-zero-order reaction (C_0-C_t=Kt) fits well the degradation of phenol with the addition of H_2O_2 (Figure 9).

The effect of different loadings of BN on TiO_2 from 0.1, 1, 2, 5, and 10% on phenol degradation in the presence of H_2O_2 is also studied (Figure 10). The phenol degradation increases with increasing BN loading on TiO_2 to reach 78.5, 82.2, and 90.6% with 0.1, 1, and 2% BN loading, respectively, within 30 min. After that, the phenol degradation decreases by 5% BN, and a continuous decrease was observed with 10% BN. This decrease in phenol degradation is attributed to the scattering of light through BNTi particles. Therefore, it can be concluded that 2BNTi is the best one for the degradation of phenol. After 30 min of using the 2BNTi photocatalyst, the TOC measurements reveal that 89% of the phenol is entirely mineralized.

With the best photocatalyst composite and keeping all experimental conditions, the same, different mass of 2BNTi was tested toward degradation of phenol (Figure 11). As we can see from Figure 11, the phenol degradation increases from 90.5, 92.7 to 94.0% with the rate of 0.79, 0.87, and 0.94× 10^{-5} M min^{-1}) with increasing the mass of catalyst from 0.1, 0.2,

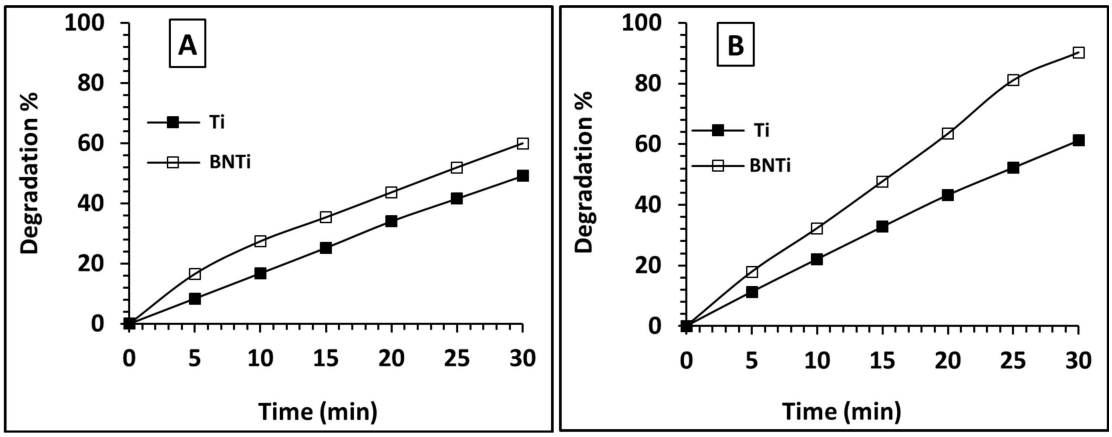

Figure 8. Degradation % of 20 ppm phenol with time on bare TiO_2 and 2BNTi (A) without the addition of H_2O_2 (B) with the addition of 70 μL H_2O_2 under 150 W Xe illumination.

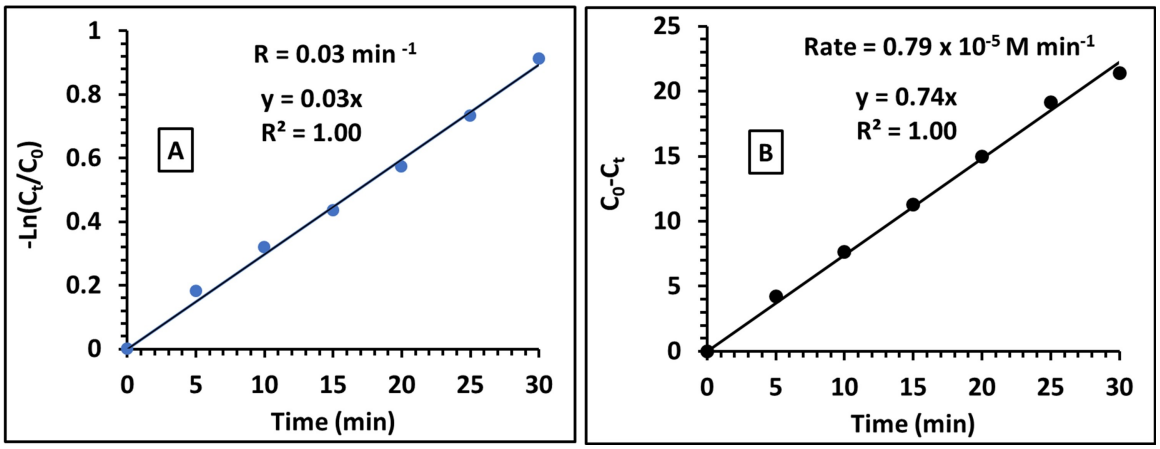

Figure 9. Rate of reaction of 20 ppm phenol with time on 2BNTi under Xe illumination (A) without the addition of H_2O_2, (B) with the addition of H_2O_2.

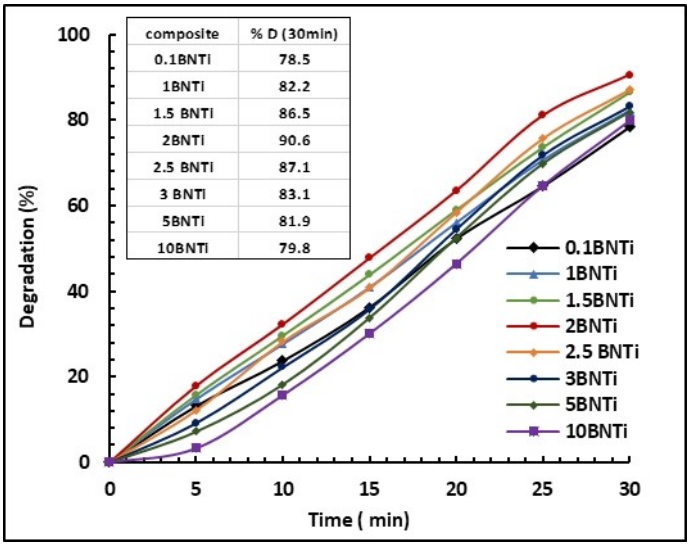

Figure 10. Degradation % (% D) of 20 ppm phenol on different concentration of on different concentration XBNTi (where X = 0.1, 1, 1.5, 2, 2.5, 3, 5 and 10 % of BN) with addition of 70 mL H_2O_2 under 150 W Xe illumination.

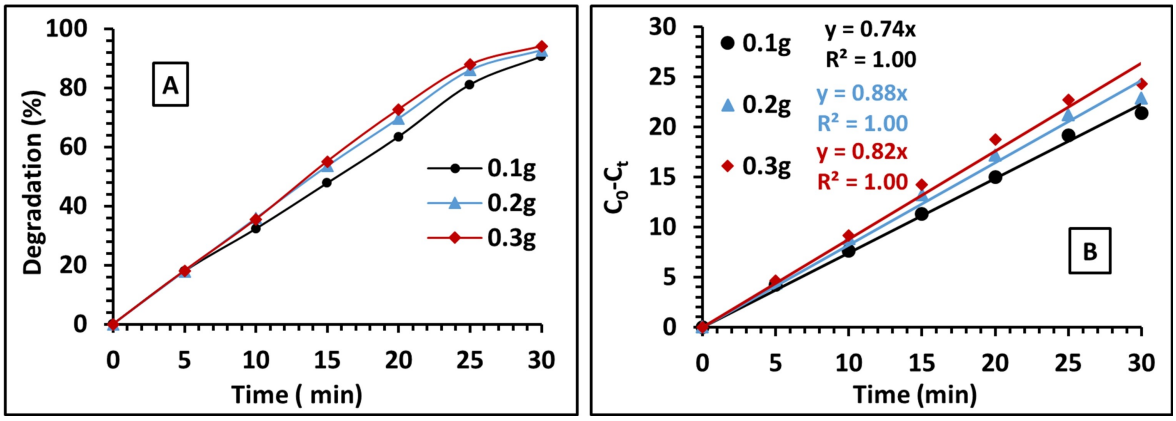

Figure 11. Degradation % (A) and rate (B) of 20 ppm phenol with time on different 2BNTi weight with the addition of 70 mL H_2O_2 under 150 W Xe illumination.

and 0.3 g BNTi. This is due to the increase of the photocatalyst's available surface area, which enhances the rate and percentage of phenol degradation.

The photocatalytic behavior of 2BNTi nanocomposite with changing the concentration of phenol is also a concern. Changing the phenol concentration from 20, 40 to 60 ppm with 0.1 g BNTi and keeping all experimental conditions the same reduces the activity of the nanocomposite sharply due to insufficient surface to degrade all phenol molecules. The degradation decreases from 90.5, 52.9, to 26.6% with 20, 40, and 60 ppm phenol, respectively. However, the reaction rate decreases slightly with increasing the initial concentration of phenol; 0.79, 0.72, and 0.65×10^{-5} M min^{-1} for 20, 40, 60 ppm phenol, respectively (Figure 12).

Photocatalytic reaction mechanism

From the above studies, it is observed that the phenol degradation improved sharply in the case of BNTi than TiO_2 under Xe illumination. This is due to the decrease in the bandgap energy of TiO_2 through the formation of the B–O–Ti bond (as proved from XPS), so the wavelength of excitation shifted from UV to the visible region. On the other hand, the huge delocalization of BN and easy transfer of electrons inhibit the rate of electron-hole pair recombination; therefore, the phenol degradation is improved sharply than in the case of TiO_2. The possible mechanism of photodegradation of phenol on BNTi in the presence of H_2O_2 can be summarized as follows:

$$TiO_2 + h\nu \rightarrow TiO_2(h^+ + e^-) \quad (3)$$

$$TiO_2\ (e^-) + BN \rightarrow TiO_2 + BN\ (e^-) \quad (4)$$

$$H_2O_2 + e^- \rightarrow {}^{\bullet}OH + OH^- \quad (5)$$

$$O_2 + e^- \rightarrow O_2^{\bullet-} \quad (6)$$

$$H_2O_2 + e^- \rightarrow {}^{\bullet}OH + {}^{\bullet}OH \quad (7)$$

$$OH^- + h^+ \rightarrow {}^{\bullet}OH \quad (8)$$

$$h^+ + H_2O \rightarrow H^+ + {}^{\bullet}OH \quad (9)$$

$$\text{phenol}/O_2^{\bullet-}/{}^{\bullet}OH/h^+/e^- \rightarrow \text{degraded products} \rightarrow\rightarrow CO_2 + H_2O \quad (10)$$

Tert-butanol (t-BuOH), p-benzoquinone (p-BQ), ammonium oxalate (AO), and $K_2S_2O_8$ (PPS-potassium persulfate) scavengers are used to capture ${}^{\bullet}OH$, $O_2^{\bullet-}$, h^+, and e^-, respectively, to clarify which species contribute more to the photocatalytic degradation of phenol on BNTi.[12] As shown in Figure 13, all four scavengers suppress the photodegradation of phenol, suggesting that ${}^{\bullet}OH$, $O_2^{\bullet-}$, h^+ and e^- contribute to the degradation of phenol. The effect of t-BuOH is slightly more noticeable than the PPS, suggesting that ${}^{\bullet}OH$ and e^- have almost similar effects on the degradation of phenol. However, the suppression is more pronounced in the case of p-BQ than AO. No degradation of phenol was observed within 30 min with the addition of p-BQ and only slight degradation of phenol after 25 min with the addition of AO. This implied that $O_2^{\bullet-}$ and h^+ play the key roles in phenol degradation under the condition studied. This observation is consistent with other research work on different photocatalysts.[12b]

Stability of the as-prepared photocatalyst

Four consecutive photocatalytic measurements under the same experimental conditions of 2BNTi nanocomposite result in the best photocatalytic activity for phenol degradation in H_2O_2 under 150 W Xe illumination was done after isolation of the photocatalyst. Figure 14 shows the bar chart of these four photocatalytic degradations with time, and the inset shows the average degradation of photocatalytic reactions with time, including the error bar. Figure 14 shows the high reliability of data, which indicates that the 2BNTi displays excellent stability and reusability.

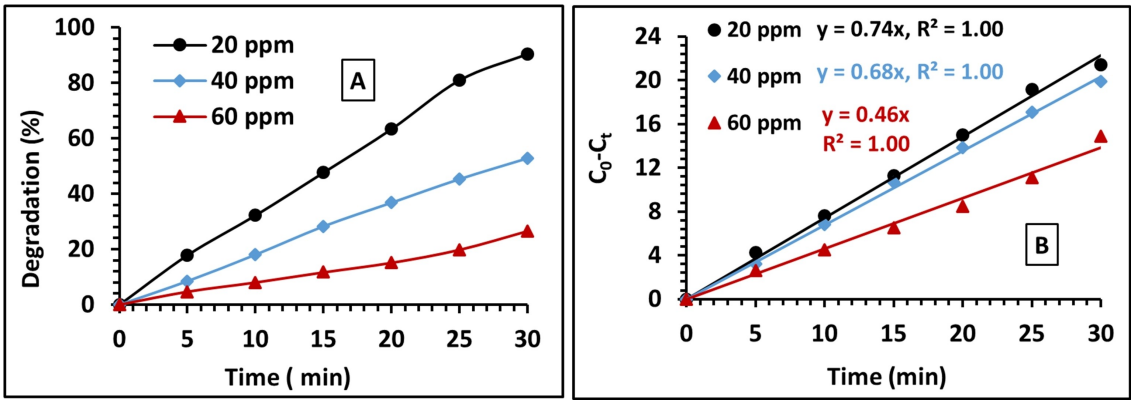

Figure 12. Degradation % (A) and rate (B) of different concentration of phenol (20, 40, and 60 ppm) with time on 2BNTi with the addition of 70 mL H_2O_2 under 150 W Xe illumination.

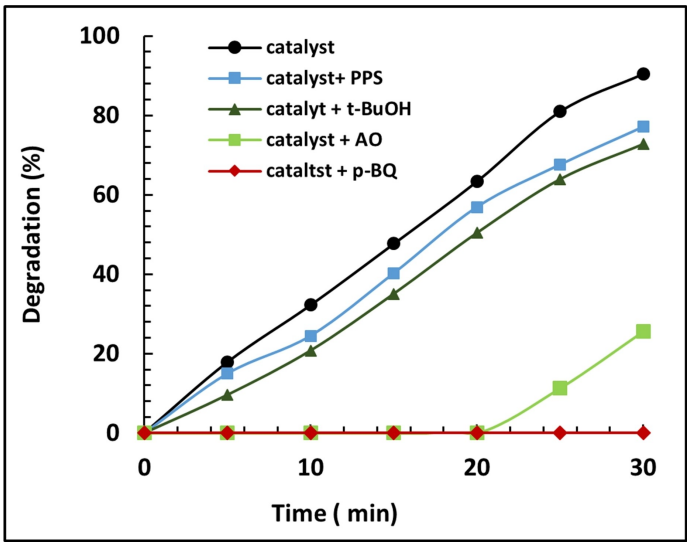

Figure 13. photocatalytic degradation of phenol on 2BNTi in the presence of PDT, t-BUOH, AO, p-BQ under Xe illumination with the addition of 70 μL of H_2O_2.

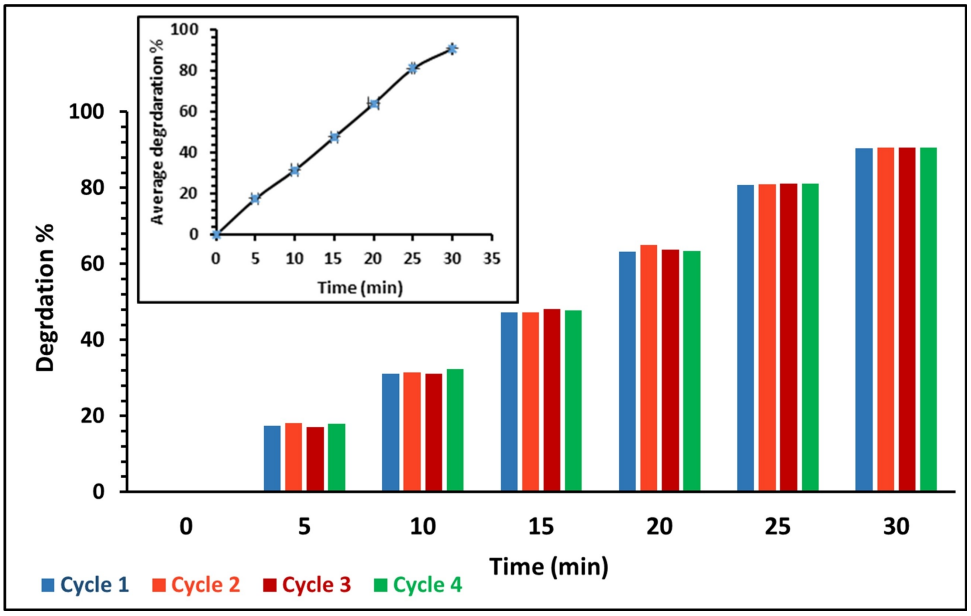

Figure 14. Stability studies of photocatalytic degradation of phenol on 2BNTi in presence under Xe illumination with the addition of 70 μL of H_2O_2.

$BNTiO_2$ nanoparticles; is it non-toxic "green"?

It is well documented that the early developmental stages of the zebrafish embryos are more sensitive to external compounds and chemicals than larval or adult zebrafish.[13] Therefore, the embryonic period of zebrafish (24 hpf and 96 hpf) is chosen as the administration time to study the possible toxicity of $BNTiO_2$ nanoparticles. At 96-hpf, the percentage of cumulative survival is measured (Figure 15A). According to the survival graph, NOCE (i.e., $<20\%$ mortality) is calculated for DEAB (PC). The NOEC for DEAB is at 1.0 μM, as this concentration of DEAB shows cumulative mortality of 12% (3 out of 25 embryos are dead), and the rest of the embryos (88%) does not show any teratogenic (morphological or physiological abnormalities) effect. According to the sigmoidal curve (Figure 15B), the LC50 values of the DEAB at five time-points for mortality with a 95% confidence limit are calculated to be 2.56 μM ($R2 \approx 0.999$). For $BNTiO_2$ treatment, a negligible mortality rate is observed at 100 mg L^{-1} concentration. However, a dose-dependent increase in the mortality rate for the embryos treated with $BNTiO_2$ at 96-hpf is observed, as shown in figure 15A. Therefore, the calculated LC50 for $BNTiO_2$ from figure 1B is 482.5 mg L^{-1}.

We selected and tested concentrations of $BNTiO_2$ nanoparticles that have environmental relevance. These concentrations are selected based on the recommendations provided by

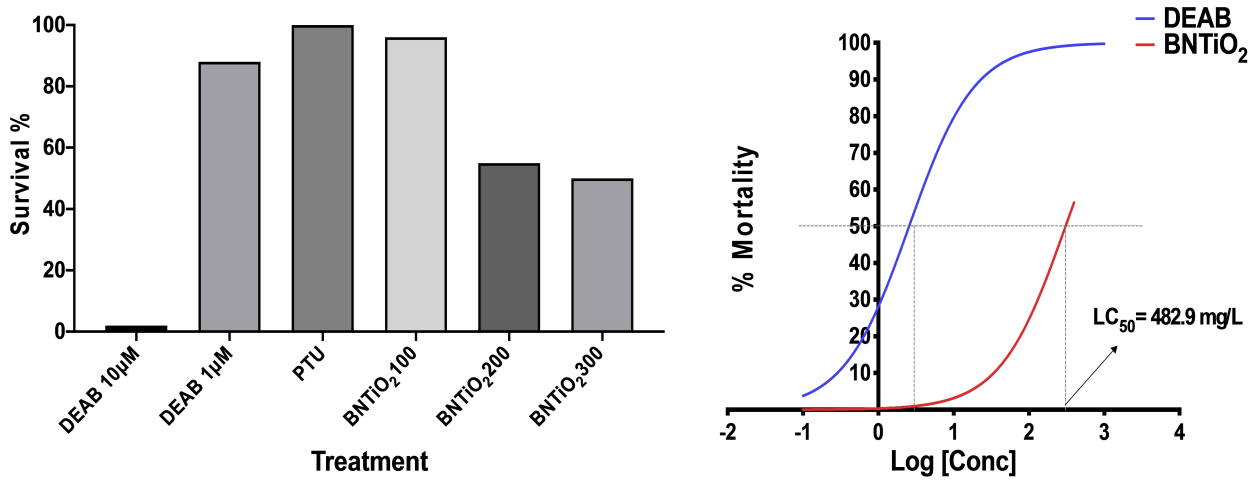

Figure 15. (A) The survival rate of zebrafish embryos at 96-hpf grown in PTU solution (Negative Control, NC), embryos treated with 1&10 mM DEAB (Positive Control, PC), and 100, 200, 300 mg L^{-1} of $BNTiO_2$ nanoparticles. (B) The mortality response curve of embryos exposed to different concentrations of DEAB and $BNTiO_2$ nanoparticles. The calculated LC50 using for DEAB is 2.56 µM, and for $BNTiO_2$ is 482.5 mg L^{-1}.

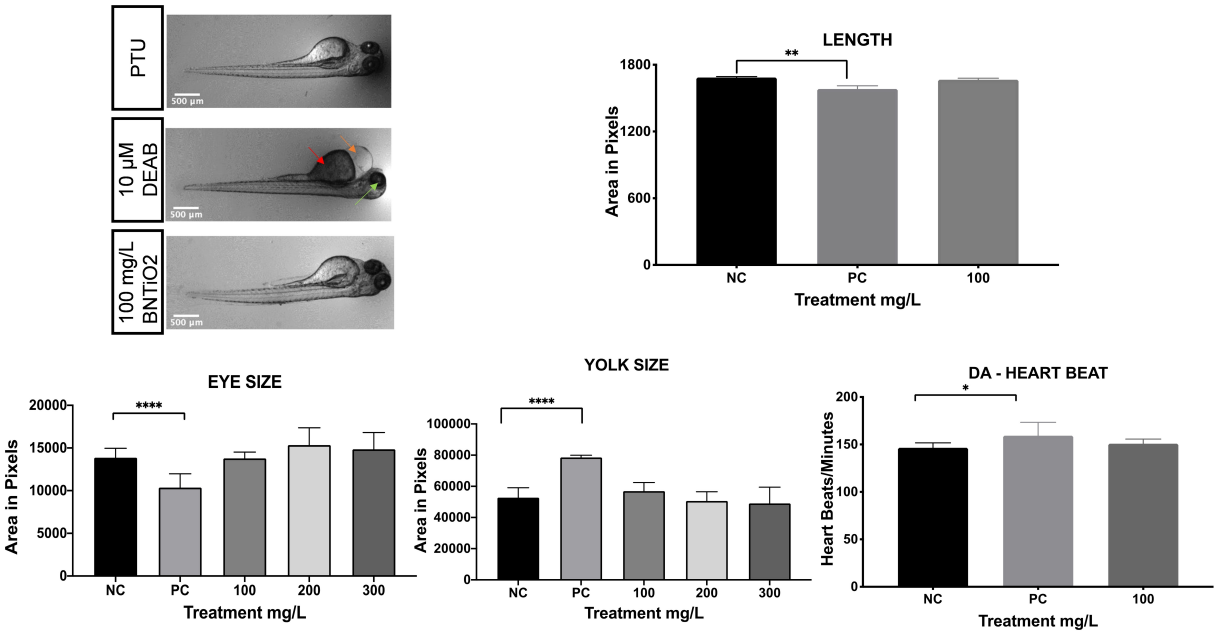

Figure 16. (A) Images representing zebrafish embryo at 96-hpf. Note the deformed embryos in DEAB: shorter size, small eye size, heart edema, and yolk edema. (B,C,D) Measurements of the average body length (B), eye size (C), yolk size (D), and (E) Heartbeats/minutes of embryos were calculated using ImageJ software version 1.52a. One-way analysis of variance (ANOVA) followed by the Dunnet test was used to compare the differences between the average of the imaged areas between groups*$p < 0.05$ and **$p < 0.01$, ****$p < 0.0001$, 10 embryos ($n = 10$) were used for each experiment.

the Fish and Wildlife Service (FWS) acute toxicity rating scale, which is classified a compound's toxicity according to LC50 as follows: highly toxic from 0.1–1.0 mg L^{-1}, 1.0–10 mg L^{-1}moderately toxic, 10–100 mg L^{-1} slightly toxic, 100–1000 mg L^{-1} practically nontoxic, and > 1000 mg L^{-1} is relatively harmless. Based on this scale, $BNTiO_2$ (LC5 = 482.5 mg L^{-1}) can be classified as practically nontoxic "green."

Quantitative Assessment of Specific Teratogenic Phenotype Exerted by $BNTiO_2$ nanoparticles

Next, the NOCE value of $BNTiO_2$ is determined, which is the minimum concentration that has no significant teratogenic or developmental effect on zebrafish embryos. For this purpose, four widely use developmental or teratogenic phenotypes are assessed, including; body length, eye size, and yolk sac size, heartbeat (beat per min) at 96-hpf. For the body, eye, and yolk size, images of the embryos are captured using HCImage

software and analyzed using ImageJ software. Compared to the NC (PTU solution), the zebrafish treated with 10 mM DEAB (PC) has a significant effect on yolk size (edema), eye size (smaller eye size), body length, and heartbeat as shown in Figure 16. However, the 100 mg L^{-1} of 2BNTiO_2 has no significant effect on any of these parameters. We cannot assess the above teratogenic parameters for any concentration of BNTiO_2 above 100 mg L^{-1}, as more than 20% of the embryos are dead before reaching the age of 96-hpf. In conclusion, the NOEC results provide another line of evidence that BNTiO_2 nanoparticles are very safe to aquatic environments when used at a concentration of less than 100 mg L^{-1}.

Conclusions

BNTi nanocomposites with different ratios between BN and TiO_2 were successfully prepared via feasible hydrothermal treatment. The 2% of BN loaded on commercially P25 TiO_2 was found to e the best composite for photocatalytic phenol degradation in the presence of H_2O_2, in which ~91% degradation was obtained within 30 min under Xe lamp-sunlight simulator. The composite showed excellent stability and reusability during four consecutive cycles. The superior activity of 2BNTi toward phenol degradation is due to lower bandgap energy, and the suppression of e−/h+ recombination resulted from synergism between BN and TiO_2 to the composite formation through the B–O–Ti bond. Therefore, 2BNTi could be considered as an excellent photocatalyst candidate for the degradation of organic compounds. Based on LC50 value and according to the Fish and Wildlife Service (FWS) acute toxicity rating scale, BNTiO_2 should be classified as "practically not toxic."

Supporting Information Summary

Experimental details are available in SI.

Acknowledgments

The authors acknowledge the Public Authority for Applied Education and Training (PAAET), Kuwait, for using their facility in the laboratory of the Department of Health Environment. This publication was partially supported by Qatar University, internal grant number QUCG-CAM-20/21-2. The findings achieved herein are solely the responsibility of the authors. Open Access funding provided by the Qatar National Library.

Conflict of Interest

The authors declare no conflict of interest.

Keywords: boron nitride · Ecotoxicology · phenol degradation · Photocatalyst · zebrafish embryo model

[1] S. B. Satpal, A. A. Athawale, *Mater. Res. Express* **2018**, *5*.
[2] a) X. Chen, C. Burda, *J. Phys. Chem. B* **2004**, *108*, 15446–15449; b) K. Eid, K. A. Soliman, D. Abdulmalik, D. Mitoraj, M. H. Sleim, M. O. Liedke, H. A. El-Sayed, A. S. AlJaber, I. Y. Al-Qaradawi, O. Mendoza Reyes, A. M. Abdullah, *Catal. Sci. Technol.* **2020**, *10*, 801–809.
[3] a) I. Tanabe, K. Matsubara, S. D. Standridge, E. Kazuma, K. L. Kelly, N. Sakai, T. Tatsuma, *Chem. Commun. (Camb.)* **2009**, 3621–3623; b) J.-J. Li, B.-L. Zhu, G.-C. Wang, Z.-F. Liu, W.-P. Huang, S.-M. Zhang, *Catal. Sci. Technol.* **2018**, *8*, 6109–6122.
[4] a) H. Al-Kandari, A. M. Abdullah, Y. H. Ahmad, S. Al-Kandari, S. Y. AlQaradawi, A. M. Mohamed, *Sci. Rep.* **2017**, *7*, 9898; b) H. Al-Kandari, A. M. Abdullah, S. Al-Kandari, A. M. Mohamed, *RSC Adv.* **2015**, *5*, 71988–71998; c) H. Al-Kandari, A. M. Abdullah, S. Al-Kandari, A. M. Mohamed, *Sci. Adv. Mater.* **2017**, *9*, 739–746; d) H. Al-Kandari, A. M. Abdullah, A. M. Mohamed, S. Al-Kandari, *ECS Trans.* **2015**, *64*, 1–12; e) H. Al-Kandari, A. M. Abdullah, A. M. Mohamed, S. Al-Kandari, *J. Mater. Sci.* **2016**, *51*, 8331–8345; f) H. Al-Kandari, A. M. Abdullah, A. M. Mohamed, S. AL-Kandari, *Int. J. Adv. Sci. Eng. & Tech.* **2016**, *4*, 62–64; g) A. M. Abdullah, N. J. Al-Thani, K. Tawbi, H. Al-Kandari, *Arab. J. Chem.* **2016**, *9*, 229–237; h) A. M. Abdullah, S. Al-Kandari, A. M. Mohamed, H. Al-Kandari, *Emergent Mater.* **2020**, *3*, 955–963.
[5] D. Liu, M. Zhang, W. Xie, L. Sun, Y. Chen, W. Lei, *Appl. Catal. B* **2017**, *207*, 72–78.
[6] a) C. Zhou, C. Lai, C. Zhang, G. Zeng, D. Huang, M. Cheng, L. Hu, W. Xiong, M. Chen, J. Wang, Y. Yang, L. Jiang, *Appl. Catal. B* **2018**, *238*, 6–18; b) Z. He, C. Kim, T. H. Jeon, W. Choi, *Appl. Catal. B* **2018**, *237*, 772–782; c) M. Nasr, R. Viter, C. Eid, R. Habchi, P. Miele, M. Bechelany, *New J. Chem.* **2017**, *41*, 81–89; d) V. Štengl, J. Henych, M. Slušná, *J. Nanomater.* **2016**, *2016*, 12; e) N. Wang, G. Yang, H. Wang, R. Sun, C.-P. Wong, *Front. Chem.* **2018**, *6*; f) J. Qu, Q. Li, C. Luo, J. Cheng, X. Hou, *Coating* **2018**, *8*, 214; g) N. S. Mishra, P. Saravanan, *ChemistrySelect* **2018**, *3*, 8023–8034; h) J. Wang, F. Ma, M. Sun, *RSC Adv.* **2017**, *7*, 16801–16822; i) C. Lee, S. Bhandari, B. Tiwari, N. Yapici, D. Zhang, Y. K. Yap, *Molecules* **2016**, *21*, 922.
[7] B. Singh, G. kaur, P. Singh, K. Singh, J. Sharma, M. Kumar, R. Bala, R. Meena, S. K. Sharma, A. Kumar, *New J. Chem.* **2017**, *41*, 11640–11646.
[8] a) H. Al-Kandari, N. Younes, O. Al-Jamal, Z. Z. Zakaria, H. Najjar, F. Alserr, G. Pintus, M. A. Al-Asmakh, A. M. Abdullah, G. K. Nasrallah, *Nanomaterials (Basel)* **2019**, *9*, 488; b) N. Younes, G. Pintus, M. Al-Asmakh, K. Rasool, S. Younes, S. Calzolari, K. A. Mahmoud, G. K. Nasrallah, *ACS Biomater. Sci. Eng.* **2019**; c) N. Younes, R. Salem, M. Al-Asmakh, T. Altamash, G. Pintus, M. Khraisheh, G. K. Nasrallah, *Ecotoxicol. Environ. Saf.* **2018**, *161*, 17–24.
[9] a) M. Zheng, Y. Gu, Z. Xu, Y. Liu, *Mater. Lett.* **2007**, *61*, 1943–1945; b) Q. Weng, Y. Ide, X. Wang, X. Wang, C. Zhang, X. Jiang, Y. Xue, P. Dai, K. Komaguchi, Y. Bando, D. Golberg, *Nano Energy* **2015**, *16*, 19–27; c) V. Štengl, J. Henych, M. Slušná, *J. Nanomater.* **2016**, *2016*, 12; d) N. Sun, Z. Xiao, *Energy Fuels* **2017**, *31*, 10186–10195.
[10] M. Hasan, A. M. Mohamed, H. Al-Kandari, *Molecular Catalysis* **2018**, *452*, 1–10.
[11] D. Liu, M. Zhang, W. Xie, L. Sun, Y. Chen, W. Lei, *Appl. Catal. B* **2017**, *207*, 72–78.
[12] a) F. Wu, X. Li, W. Liu, S. Zhang, *Appl. Surf. Sci.* **2017**, *405*, 60–70; b) J. Yao, H. Chen, F. Jiang, Z. Jiao, M. Jin, *J. Colloid Interface Sci.* **2017**, *490*, 154–162; c) W. Zhao, Z. Wu, H. Shi, D. Wang, *J. Photochem. Photobiol. A* **2005**, *171*, 97–106.
[13] K. Rasool, G. K. Nasrallah, N. Younes, R. P. Pandey, P. Abdul Rasheed, K. A. Mahmoud, *ACS Sustainable Chem. Eng.* **2018**, *6*, 3896–3906.

Submitted: December 28, 2020
Accepted: May 5, 2021